# Membrane fluctuations mediate lateral interactions between cadherin bonds

Susanne F. Fenz*,[1,2] Timo Bihr*,[3,4] Daniel Schmidt*,[3] Rudolf Merkel,[2] Udo Seifert,[4] Kheya Sengupta,[5] and Ana-Sunčana Smith[3,6]

[1]*Department of Cell and Developmental Biology, Universität Würzburg, Am Hubland, 97074 Würzburg, Germany*

[2]*Institute of Complex Systems 7: Biomechanics Forschungszentrum Jülich GmbH, 52425 Jülich, Germany*

[3]*PULS Group, Institut für Theoretische Physik and the Excellence Cluster: Engineering of Advanced Materials, Friedrich-Alexander-Universität Erlangen-Nürnberg, Nägelsbachstrasse 49b, 91052 Erlangen, Germany*

[4]*II. Institut für Theoretische Physik, Universität Stuttgart, Pfaffenwaldring 57, 70550 Stuttgart, Germany*

[5]*Aix-Marseille Université, Centre Interdisciplinaire de Nanosciences de Marseille, CNRS UMR 7325, Campus de Luminy, 13288 Marseille cedex 9, France*

[6]*Institute Ruđer Bošković, Division of Physical Chemistry, Bijenička cesta 54, 10000 Zagreb, Croatia*

# Abstract

The integrity of living tissues is maintained by adhesion domains of *trans*-bonds formed between cadherin proteins residing on opposing membranes of neighboring cells. These domains are stabilized by lateral *cis*-interactions between the cadherins on the same cell. However, the origin of *cis*-interactions remains mysterious since they are detected only in the context of *trans*-bonds. By combining experimental, analytical and computational approaches, we identify bending fluctuations of membranes as a source of long-range *cis*-interactions, and a regulator of *trans*-interactions. Nanometric membrane bending and fluctuations introduce cooperative effects that modulate the affinity and binding/unbinding rates for *trans*-dimerization, dramatically affecting the nucleation and growth of adhesion domains. Importantly, this regulation relies on physical principles and not on details of protein-protein interactions. These omnipresent fluctuations can thus act as a generic control mechanism in all types of cell adhesion, pointing to the so-far unclear physiological significance of recently identified active fluctuations of cellular membranes.

Cadherins are a family of transmembrane proteins responsible for cohesion of cells [1, 2]. Following formation of membrane-bridging *trans*-dimers, they assemble into domains at the cell-cell interface, presumably *via* lateral *cis*-interactions [3], ultimately connecting the actin cytoskeletons of neighbouring cells [4–7]. Cells containing a specific cadherin subtype cluster together to the exclusion of other types, both in cell culture and during embryo development [8]. This selectivity is promoted by small variations in the two-dimensional binding affinity (2D-$K_a$) for *trans*-dimerization [3, 9], which allows proteins of the cadherin family to have a structural and regulatory role in tissue morphogenesis, homoeostasis [10] and malignancy: E-cadherins in particular serve as suppressors of cancer invasion and metastasis [11, 12].

Cadherins exhibit a considerable level of complexity even at the level of single *trans*-bond [13–15] that usually links the opposing outermost extracellular-domains [16–18]. *Trans*-interactions have been studied in detail and recently the factors governing their stability were elucidated [18]. Experiments have also established the importance of *inplane* clusters, whose initial formation and renewal occur in three steps: spontaneous recruitment to form a domain, lateral growth and finally, active release from the resulting cluster [19–23]. In spite of these advances, the origin of *cis*-interactions that lead to *in plane* clustering remains elusive. Specifically, *cis*-interactions have only been encountered in *trans*-bound molecules and have never been detected in solution. Short-range *cis*-interactions of molecular origin were shown to be critical for formation of well-ordered cadherin arrays [19, 24] which are important for actin assembly [6] and adhesion stabilization, but such interactions do not explain why cadherins cluster only while participating in *trans*-interactions between two membranes. Recent ground-breaking computational studies implicate entropic reasons related to the mechanics of the monomeric and dimeric states [3, 25], which may indeed organize already clustered cadherins, but again, they alone cannot explain the exquisite sensitivity of the cadherin system to membrane parameters as hinted at in recent experiments [12].

Here we set-up *in vitro* and *in silico* cell-free models in the form of giant unilamellar vesicles (GUV) decorated with freely diffusing E-cadherin (E-cad) extracellular-domains, and complementary supported lipid bilayers (SLB) which are equivalently functionalized [26] (Fig. 1). These models capture the essence of the molecular recruitment and domain growth phases described for cells. We demonstrate decisively that cadherin domain formation is indeed strongly regulated by membrane parameters. We link these observations to our analytical calculations that pinpoint membrane-fluctuation transmitted cooperativity as not

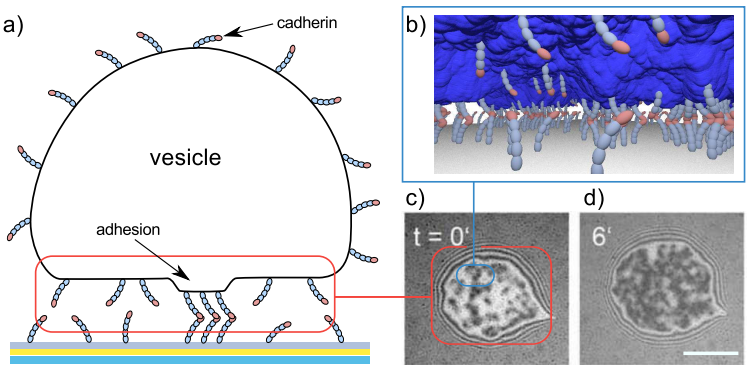


Figure 1: The model system for cell-cell adhesion. a) Schematic representation depicting E-cad functionalized GUV and SLB. b) The key players, including the fluctuating GUV membrane (blue) and the SLB (gray), both enriched with mobile E-cad fragments (gray-orange beads), are incorporated into a coarse-grained simulation that can accurately reproduce the adhesion dynamics. c) and d) Snapshots of the GUV/SLB interface imaged in RICM. The interface, called the contact zone, is seen as an area of mixed dark and bright pixels (see flickering in corresponding dynamic movie shown in the Supplementary Information), surrounded by well-defined quasi-continuous interference fringes from the uniformly gray background. Dark areas (suppressed flickering) within the contact-zone are *trans*-bond domains. The scale bar is 10 $\mu$m.

only a significant modulator of 2D-$K_a$ for both *trans*- and *cis*-dimerization, but also capable of promoting *cis*-interactions by itself leading to the formation of non-ordered domains.

In our experiments, a population of GUVs with either strong or weak membrane fluctuations is obtained by variation of osmotic difference between the inner and outer buffers. The GUVs first hover over SLBs, spreading to establish a contact zone in the unbound state. Next, E-cads on the opposing membranes interact and form adhesion domains corresponding to the bound state (see Fig. 1). The GUV/SLB interface is imaged dynamically in reflection interference contrast microscopy (RICM) [27–29], and the time dependent inter-membrane distance $h$ is measured, enabling quantification of membrane fluctuations $\xi_\perp^0$ and the average inter-membrane separation $h_0$ in the unbound state, the analysis of adhesion-morphology in the bound state and identification of the growth-dynamics of the entire process. (see Supplementary Information for details of experiments/data-analysis and for dynamic data). In the GUV population, $h_0$ is seen to vary in the range 75 nm and 110 nm and $\xi_\perp^0$ from 5 nm to 20 nm. Such a spread occurs even within a single vesicle preparation as previously observed in equivalent systems [30], where no "bound" state ever takes place (control experiments in [26] and SI).

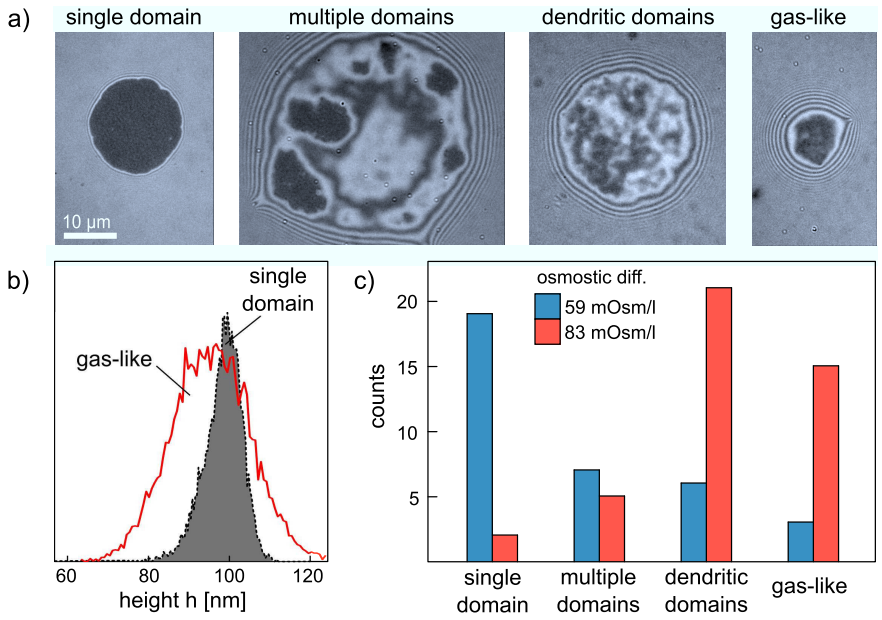


Figure 2: The morphology of adhesion domains in the steady state depends parameters describing the unbound state, namely the separation $h_0$ between the vesicle membrane and the substrate, and the fluctuations amplitude of the vesicle membrane $\xi_\perp^0$. a) RICM images of contact-zones in the bound state showing the four characteristic morphologies of the adhesion domains. The scale bar is 10 $\mu$m. b) Probability distribution of the measured inter-membrane separation in the unbound state for GUVs that eventually display gas-like domain (red, mean separation $h_0 = 95\,\text{nm}$ and fluctuation amplitude $\xi_\perp^0 = 10\,\text{nm}$) or single domain (black, $h_0 = 98\,\text{nm}$ and measured $\xi_\perp^0 = 3.5\,\text{nm}$). Extraction of true from measured fluctuation amplitudes (17 nm for gas-like and 12 nm single domains) is described in the SI. c) Distribution of domain morphology in GUV populations prepared under conditions of large (red) or small (blue) osmotic differences. Large osmotic difference (stronger fluctuations, 43 GUVs) yields more dendritic-like domains due to faster nucleation, whereas low osmotic differences (lower fluctuations, 35 GUVs) promote radial growth of a single domain.

Four characteristic types of steady-state adhesions are identified based on morphological analysis of the bound state: single, multiple, dendritic, or gas-like domains (Fig 2a). These morphological states are correlated with corresponding unbound state parameters $h_0$ and $\xi_\perp^0$ (Fig. 2b). Nucleation and growth of one (or few) domains are preferred at smaller osmotic difference with low membrane fluctuations (Fig. 2c, blue bars). At the large osmotic difference, stronger fluctuations (Fig. 2c, red bars) clearly facilitate nucleation leading to dendritic and gas-like domains.

We infer that the properties of the unbound state couple directly to the final organization of *trans*-dimers and to the dynamics of growth. Detailed analysis (Fig. 2c) shows that increase of fluctuations by a few nanometres may drive the system from the regime of large

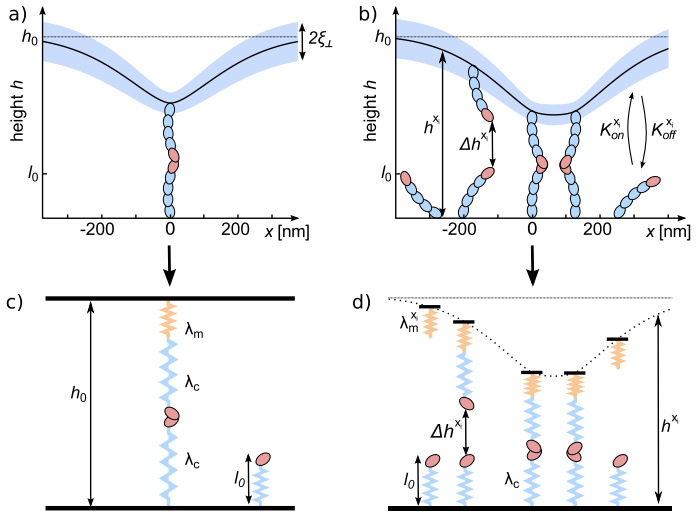


Figure 3: Modeling the coupling between shape and fluctuations of the membrane and cadherin cluster formation. a) Calculated average shape (black solid curve) of a membrane deformed by an isolated *trans*-dimer, for the experimental membrane rigidity $\kappa = 20\,\mathrm{k_B T}$ and the fluctuation amplitude in the unbound state of $\xi^0_\perp = 10\,\mathrm{nm}$, implying lateral correlation length $\xi_\parallel = 120\,\mathrm{nm}$. The deformation extends about 500 nm around the bond. Shaded area around the membrane represent the distance-dependent fluctuation amplitude $\xi^{x_i}_\perp$. b) Membrane profile and fluctuations around two cadherin *trans*-dimers separated by $\xi_\parallel$. Bonds are formed with a rate $K^{x_i}_{\mathrm{on}}$ and broken with a rate $K^{x_i}_{\mathrm{off}}$ depending on the local inter-cadherin separation $\Delta h^{x_i}$ and the fluctuations $\xi^{x_i}_\perp$ at the position of the $i$-th binder. c) Mapping the single bond system into coupled thermalized springs. The yellow ($\lambda_m$) and the blue springs ($\lambda_c$) represent the membrane and the cadherin molecules, respectively. d) In the case of several bonds, the membrane is parametrized by a spatially and temporally variable spring constants $\lambda^{x_i}_m$, and separations $\Delta h^{x_i}$, reflecting its the local shape and fluctuations .

radially growing single domain to a regime where numerous very small domains are formed simultaneously. Similarly, nanometric increase in the separation between membranes results in less numerous adhesion domains which become larger in time.

Such a sensitive dependence of the entire adhesion process on initial $h_0$ and $\xi^0_\perp$ clearly points to a regulatory role of the membrane in determining the *trans*- and *cis*-dimerization. This phenomenon can be understood by recognizing that the formation of a *trans*-dimer induces local deformations (Fig. 3a) and suppression of membrane fluctuations. We hypothesize that these changes in the membrane configuration and dynamics enhance *trans* bonding between cadherins, effectively leading to *cis*-interactions that induce aggregation of the laterally mobile cadherins into *inplane* domains (Fig. 3b). Note that the range of such membrane-mediated *cis*-interactions correspond to the extent of the deformation fields of its shape and the fluctuations. This range is governed by the lateral correlation length of

the membrane $\xi_\parallel$ [31, 32]. For a single *trans*-bond its lower bound is at zero tension, where it is set by the bending rigidity $\kappa$ and $\xi_\perp^0$ ($\xi_\parallel = \xi_\perp^0\sqrt{8\kappa/(k_BT)}$; $k_B$ being the Boltzmann constant, and $T$ the temperature). The calculated shape in Fig. 3a shows that the interaction field in fact extends to about $4\xi_\parallel$. For the current experimental conditions, this is at least 500 nm, leading to long-range interactions. These membrane-mediated *cis*-interactions are complementary to direct, short-range *cis*-interactions responsible for the formation of the orderly cadherin arrays within adhesion domains [19, 24].

To support this hypothesis, we construct a mechanistic model (Fig. 3c), where the cadherins are represented by harmonic, thermalized springs (elastic constant $\lambda_c$, length $l_0$), attached either to a flat (SLB), or to a fluctuating deformable (GUV) membrane. The latter is mapped to a spring with an elastic degree of freedom, whose local effective elastic constant is $\lambda_m^{x_i} \equiv k_BT(\xi_\perp^{x_i})^{-2}$ ( $\xi_\perp^{x_i}$ being the fluctuation amplitude of the membrane at the position of the cadherin $x_i$ [33]). In the absence of any bonds $\lambda_m^{x_i} = \lambda_m$ is position independent. The *trans*-interaction is represented by a potential well, of range $\alpha$ and depth equal to the 3D binding affinity $\epsilon_b = 7\,\mathrm{k_B T}$ [3]. No explicit short-range direct *cis*-interactions are introduced in order to clearly isolate the effects of membrane-mediated long-range interactions. In this description (derivation in SI section IIA), the local free energy gain $E_b^{x_i}$ for forming a *trans*-dimer at lateral position $x_i$ is:

$$E_b^{x_i} = \frac{1}{2}\Omega_u^{x_i}(\Delta h^{x_i})^2 + \frac{1}{2}\ln\left[\frac{2\pi}{\Omega_u^{x_i}\alpha^2}\right] - \epsilon_b. \tag{1}$$

The first term is the deformation energy stored in the *trans*-dimer and the membrane. It is proportional to the effective spring constant $\Omega_u^{x_i}$ of a construct made of three springs in series (the two cadherins and the membrane) and to $(\Delta h^{x_i})^2$, where $\Delta h^{x_i} \equiv h_0^{x_i} - 2l_0$ is the extent to which the construct needs to stretch in order to bring the two cadherins into binding range, $h_0^{x_i}$ being the vertical distance between the two membranes at $x_i$ before the bond is formed and $l_0$ the size of E-cad (see Fig. 3d). The second term on the right hand side of eq. (1) is the entropic penalty associated with the suppression of the membrane as well as cadherin conformational fluctuations. An estimation of the value of the two terms shows that they are comparable for realistic experimental parameters (section II in SI).

The long-range nature of the membrane-mediated interactions is the source of many body effects and hence, correlations between *trans*-dimers. If membrane-transmitted correlations

are weak, then $\Omega_u^{x_i}$ and $\Delta h^{x_i}$ do not depend on the position $x_i$ and formation of each *trans*-dimer is an independent event. However, when these correlations are strong, as for the current experiments and in typical cellular systems [7, 34], the binding or unbinding of one *trans*-dimer affects all others in its vicinity (Fig. 3d). The free energy gain for the formation of the *trans*-dimer $\tilde{E}_b^d$, i.e., the ensemble 2D binding affinity, becomes

$$\tilde{E}_b^d = \frac{1}{N_b} \sum_{i=1}^{N_b} \left( E_b^{x_i} + \frac{1}{2} \ln \left[ \frac{\lambda_m + \lambda_c}{\lambda_m^{x_i} + \lambda_c} \right] \right), \tag{2}$$

where $N_b$ is the number of formed bonds (derivation in SI section IIB). The second term arises from non-local entropic costs for suppressing the fluctuations in the entire system. Importantly, eq. (2) shows that the affinity $\tilde{E}_b^d$, which is defined at the level of the ensemble, depends on the actual distribution of bonds and therefore, is meaningful only in steady state and even then it depends on the properties of the membrane.

Going beyond the above static description, understanding the dynamics requires modeling the binding and unbinding rates $k_{\text{on}}(h)$ and $k_{\text{off}}(h)$ [35–37]. As clarified by Bell in 1978, these rates depend on the instantaneous separation $h$ between the cadherins, which obviously do not interact at separations beyond the binding range. For cadherins embedded into simple static interfaces, $k_{\text{on}}(h)$ and $k_{\text{off}}(h)$ are expected to obey local detailed balance [37]. Membranes undergo fast stochastic motions, which can be characterized by a Gaussian height distribution function $p^{x_i}(h)$, with the first and the second moments being the average height $h_0^{x_i}$ and the fluctuation amplitude $\xi_\perp^{x_i}$ [30, 39, 40]. The amplitude of these fluctuations determines how often the cadherins get into binding range, and how strong the stochastic forces acting on a bond are. Therefore, in order to obtain the actual effective rates for the *trans*-dimerization $K_{\text{on}}^{x_i}$, $K_{\text{off}}^{x_i}$, the height-dependent rates are weighed by the membrane height distribution function $p^{x_i}(h)$

$$K_{\text{on/off}}^{x_i} \equiv \int \mathrm{d}h \, p^{x_i}(h) k_{\text{on/off}}(h), \tag{3}$$

Consequently, the effective reaction rates ($K_{\text{on}}^{x_i}$, $K_{\text{off}}^{x_i}$) depend directly on $\Delta h^{x_i}$ and $\xi_\perp^{x_i}$ at a given position on the membrane (see Fig. 4 and SI section III). The clear separation in time scales between the membrane fluctuations and the binding kinetics ensures that $p^{x_i}(h)$ is fully sampled and that the averaging is appropriately performed.

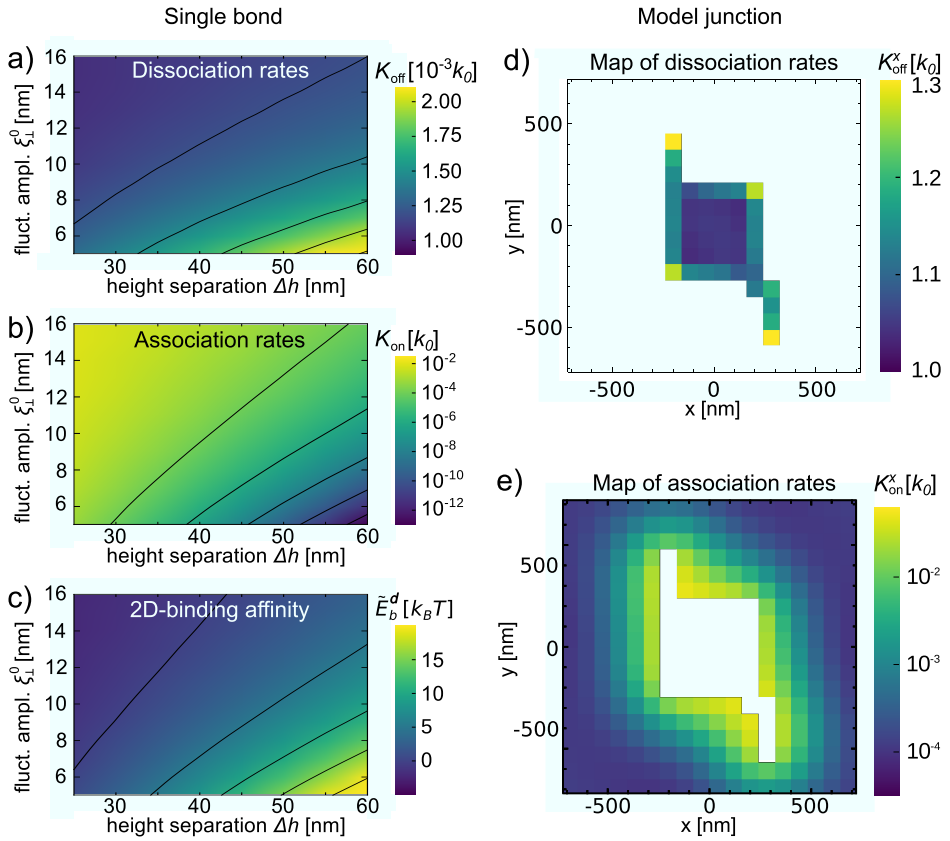


Figure 4: Effective rates (in units of the intrinsic reaction rate $k_0$) and affinity (in units of $k_BT$) for *trans*-dimerisation and *cis*-cluster formation. a) Dissociation rate $K_{\text{off}}$, b) association rate $K_{\text{on}}$ and c) effective 2D-binding affinity $\tilde{E}_b^d$ for an isolated *trans*-dimer as a function of the initial membrane separation $h_0$ and fluctuations $\xi_\perp^0$. While $K_{\text{off}}$ evolves slowly, $K_{\text{on}}$ changes by several orders of magnitude in the studied parameter range. d) Map of $K_{\text{off}}$ depending on the position of a bond within a model junction (the magnitude is mapped according to the color bar). e) Map of $K_{\text{on}}$ for free binding sites around a model junction. In the calculations, the membrane has $\kappa = 20\,\text{k}_\text{B}\text{T}$ and the harmonic springs corresponding to the cadherins have a stiffness $\lambda_c = 5 \times 10^{-2}\,\text{k}_\text{B}\text{T}/\text{nm}^2$ with binding affinity $\epsilon_b = 7\,\text{k}_\text{B}\text{T}$. In d) and e) $h_0 = 40\,\text{nm}$ and $\xi_\perp^0 = 10\,\text{nm}$.

For an isolated *trans*-dimer, the unbinding rate increases with fluctuations because stronger fluctutions exert larger stochastic forces inducing unbinding, but fluctuations also promote binding because the probability of encounter between the two cadherins is increased (Fig. 4a-b). Overall, the effect of fluctuations on $K_{\text{on}}^{x_i}$ is larger than on $K_{\text{off}}^{x_i}$, which suggests that membrane fluctuations stabilize *trans*-dimers. This is reflected in the 2D affinity for a single bond, which changes substantially with small changes in $h_0$ and $\xi_\perp^0$. This is shown in Fig. 4c, where negative values reflect an energetically stable bond.

Due to membrane-mediated correlations, the effective rates are not uniform within and

around a junction. Instead, they are sensitive to the immediate neighborhood of each bond. Specifically, deep within a cluster, where each cadherin complex is surrounded by other *trans*-dimers, the unbinding rate is small (Fig. 4d). It is 30% larger for bonds at a smooth edge of the cluster then for bonds in the center, while the bonds at a corner or isolated *trans*-dimers are even more unstable. Similarly, compared to cadherins far away from the cluster, where the binding probability is very low, free cadherins at the edge of the cluster have up to four orders of magnitude larger probability to form a bond, (Fig. 4e), which again points to a subtle interplay of *trans*- and membrane-mediated *cis*-interactions.

Naturally, the susceptibility of the reaction rates to the membrane parameters is reflected in the nucleation dynamics of adhesions. One key parameter characterizing the nucleation is the number of *trans*-dimers $N_c$ forming the smallest stable adhesion domain. Within the capillary approximation [41], $N_c \simeq 1 + \frac{(\Delta h)^4 \lambda_m^2}{4\pi\rho_b \xi_{||}^2 \left(\tilde{E}_b^d\right)^2}$, where $\rho_b$ is the bond density within the adhesions junction. The minimal number of *trans*-dimers within a stable junction is typically small [41, 42]. It increases with the fourth power of the separation between the unbound cadherins, and decreases with the fourth power of the membrane fluctuation amplitude.

The second key parameter is the average nucleation time $\bar{\tau}$, which is directly related to effective rates for the association and dissociation of the first and the second bond. In the regime of moderate fluctuations, the nucleation time is a decreasing exponential function of the square of the fluctuation amplitude, and an increasing exponential function of the square of the initial separation between cadherins.

This predicted extreme sensitivity of both the critical size and the characteristic nucleation time further emphasizes the importance of the membrane parameters for the formation of model junctions. Moreover, it is fully consistent with the experimentally observed variability of the number and size of growing adhesions junctions due to very small variations in the GUV membrane fluctuation amplitude, as well as in the initial height separation between the GUV and the SLB (Fig. 2).

To verify this analytic theory in the parameter range characteristic for the experimental conditions, we take advantage of a recently developed coarse-grained Monte Carlo (MC) simulation framework [37]. We simulate an entire GUV binding to an SLB (both $1000\,\mu\mathrm{m}^2$), with the spatial and time resolutions of 40 nm and $5 \times 10^{-6}$ s for about 100 s or until equilibrium is reached (SI section III). Binding is promoted by cadherins, present at experimental concentrations. The diffusion constant of free cadherins was estimated from previously mea-

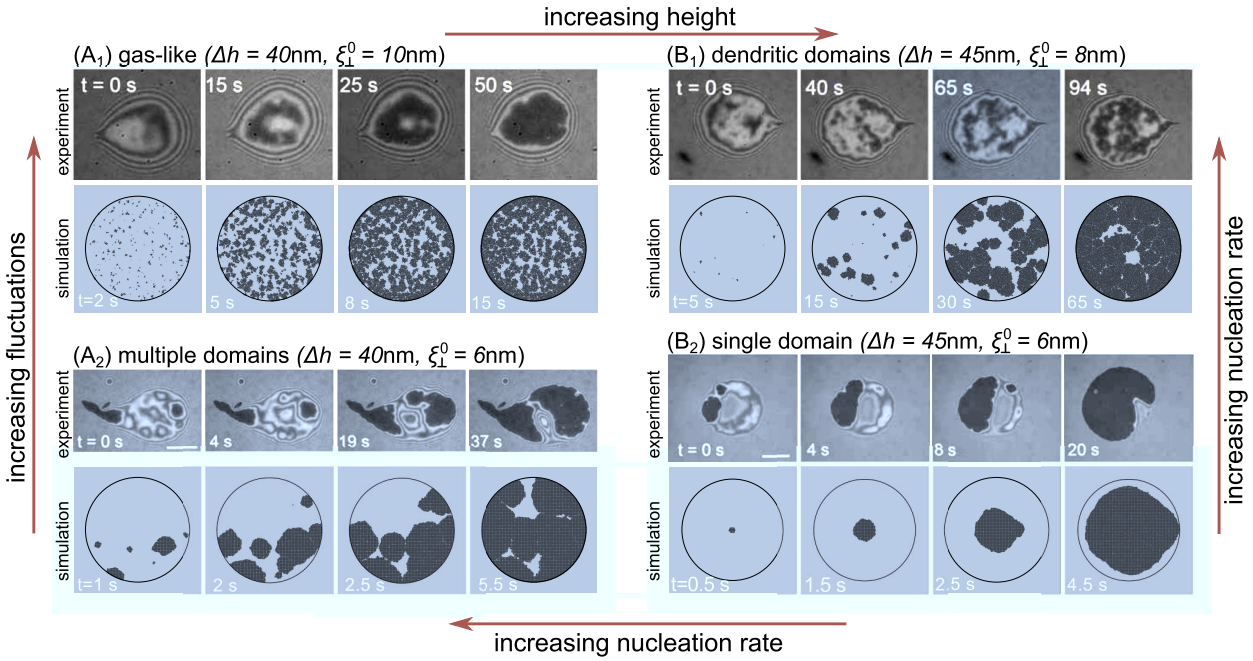


Figure 5: Comparison of growth dynamics of cadherin adhesions in experiments and matching Monte Carlo simulations. In each panel, RICM images are at the top, and simulations are at the bottom. Examples of vesicles that ultimately exhibit one of the four characteristic domain types: ($A_1$) gas-like domain, ($B_1$) dendritic domains, ($A_2$) multiple domains, and ($B_2$) radial growth single domain. The average distance between cadherins on the two unbound membranes ($\Delta h$) and the average fluctuation amplitude ($\xi_\perp^0$) as set in the simulations are indicated above each panel. Full characterization of the experimental systems is given in the SI.

sured values of lipid-anchored proteins diffusing in a model membrane [26]. The formation of *trans*-dimers is governed by rates introduced in Eq. (3), and is associated with the loss of mobility of the otherwise mobile cadherins. For a complete list of the simulation parameters see SI. As shown by the comparison of the measured (top sequences) and simulated (bottom sequences) adhesion dynamics (Fig. 5), all four regimes of growth (gas-like $A_1$, dendritic domains $B_1$, multiple domains $A_2$ and a single domain $B_2$) are reproduced in the absence of direct *cis*-interactions. Notably, spontaneous formation of domains is observed under appropriate conditions.

The overall results of simulations are, moreover, summarized in phase diagrams (Fig. 6a-b, Fig. SI-1). Consistently with measurements presented in Fig. 5 (denoted in Fig. 6a-b with letters placed in appropriate positions), growth regimes (symbols in Fig. 6a) continuously change as the 2D affinity of the ensemble changes for about $4\,k_BT$ over the investigated parameter range (background of Fig. 6a). This change of affinity is the direct

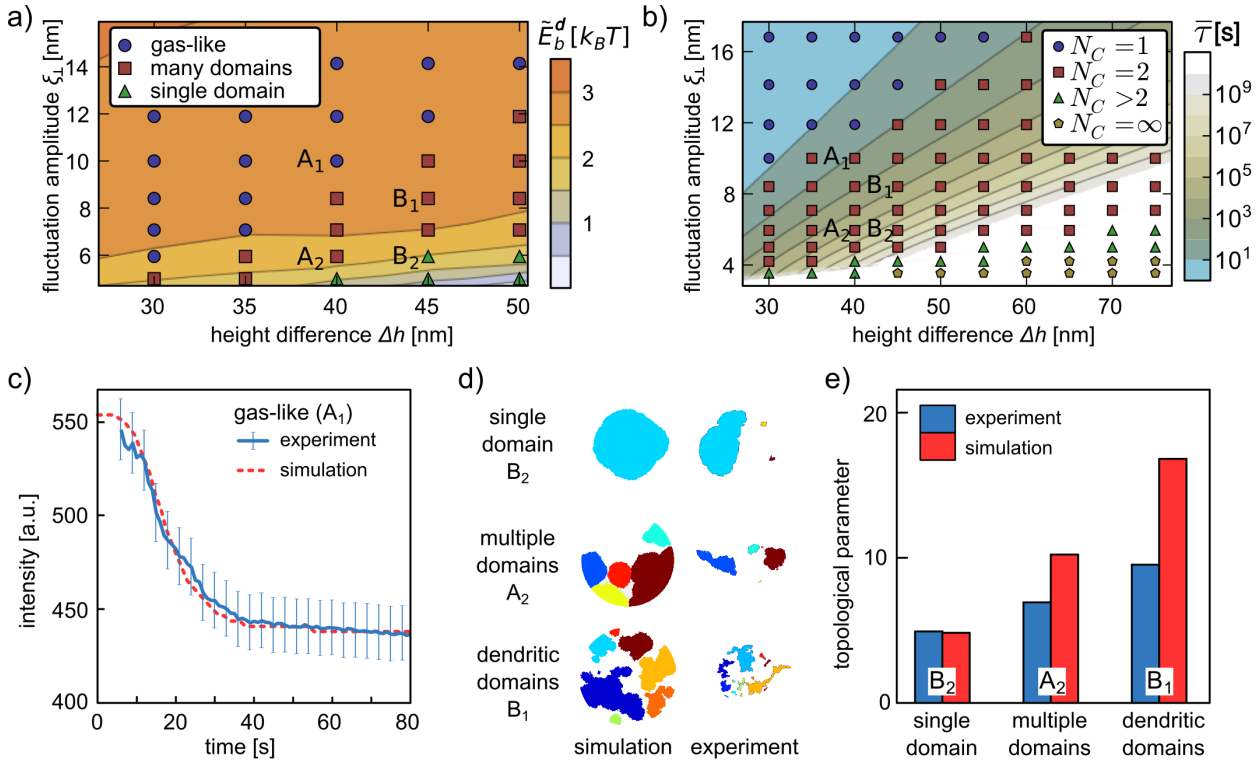


Figure 6: Comparison of experiments and simulations. a) Map of the 2D binding affinity as determined from steady state distributions of bonds using the same parameters as in Fig. 5. The result is overlaid with symbols denoting the type of domain growth (gas-like, dendritic, multiple and a single domain). Experimental data points corresponding to the four vesicles from Fig. 5 are indicated. b) Parameters determining the nucleation. The colored background represents the mean nucleation time $\bar{\tau}$, while the symbols mark the number $N_c$ of *trans*-dimers necessary to form a stable seed. c) Evolution of the measured intensity from RICM indicating the mean height of the contact zone as the adhesion process proceeds for a vesicle of type $A_1$. The error bars associated with measurement of the height dependent intensity $I \pm \Delta I$ arises from shot noise, and hence, $\Delta I = 0.7 * \sqrt{I}$. The detector specific factor is determined from calibration measurements [38]. Comparison with experiments is obtained by fitting the intrinsic reaction rate $k_0$ used in simulations as a free parameter. For the particular vesicle, $h_0 = 95\,\text{nm}$ and $2l_0 = 52\,\text{nm}$ (see SI section ID). d) Individual domains shown in different colors (left: simulations in red, right: experiments in blue) for radial growth ingle domain (top row), multiple domains (middle row), and dendritic domains (bottom row). e) The topological parameter defined as $C/\sqrt{A}$ ($C$ is total edge length and $A$ is total adhered area). For comparison with experiments, the resolution of the contact zone obtained from simulations was downsized to the experimental resolution.

cause of the variability in the number of bonds forming the stable seed and is reflected in the mean nucleation time (Fig. 6b).

For small separations and strong fluctuations ($A_1$ in Figs. 5 and 6), the formed bonds

are sparsely distributed over the entire contact zone in a gas-like fashion. As time passes, their density gradually increases before reaching a steady-state. This is seen as a continuous decrease followed by the saturation of the mean height of the membrane in contact zone as a function of time (Fig. 6c). For these conditions the long-range correlations between *trans*-dimers are very weak. Single bonds are stable ($N_c = 1 - 2$ as shown by symbols in Fig. 6b), and the nucleation time is very short (background of Fig. 6b).

Decreasing the fluctuations amplitude ($A_2$ in Figs. 5 and 6) or increasing the separation ($B_1$) results in the coarsening of the growth process. This is associated with the appearance of small domains, densely populated with cadherin constructs (dark spots with suppressed fluctuations in RICM). The number of bonds forming the stable seed increases ($N_c = 2$), but at the same time, the *cis*-interactions strengthen too. Consequently, bonds start to form domains which grow and ultimately merge into dendritic structures (Fig. 6d). Their morphology is characterized by a large topological parameter defined as the ratio of circumference to the square root of the area (Fig. 6e, analysis summarized in SI section IVD).

Further decreasing the fluctuation amplitude and separating the membranes in the unbound state by 5 nm compared to $A_1$, favors formation of a single, radially expanding domain ($N_c \geq 2$) with tightly packed bonds ($B_2$ in Figs. 5 and 6). This is the consequence of strong, membrane-induced *cis*-interactions which drive the formation of nearly circular domains as evidenced by the small values of the topological parameter. Furthermore and perhaps equally relevant is the agreement between experimental results and the predicted increase in the nucleation time of several orders of magnitude compared to the conditions in $A_1$ (background of Fig. 6b).

Our investigation shows that thermally induced membrane fluctuations can introduce long-range *cis* interactions between bonds on model membranes, resulting in very sensitive dependence of the entire adhesion process on inter-membrane separation and strength of undulations. Importantly, the same effect occurs in cells where fluctuations are active - driven by actin polymerization dynamics [39, 40]. In fact, protrusions and retractions of filopodia, which are a source of fluctuations have recently been found necessary for the initiation of cadherin junctions [12]. Naturally, disruption of actin polymerization prevents adhesion [34]. However, at the early stages of adhesion, cadherin *trans*-dimers are mobile [44], suggesting that association with actin is not important for initial cadherin recruitment [43].

On the other hand, there is a strong evidence of the involvement of the membrane in the early formation of adhesions. Specifically, it was already observed that E-cadherin accumulation depends on transient activation of phosphatidylinositol 3-kinase and Rac1, the latter intensifying membrane fluctuations. Upon the formation of tightly packed contacts fluctuations (and the Rac1 activity) are suppressed to stabilize the weak cadherin binding [43].

Our work also shows that fluctuations can control the size, as well as the density of bonds within a domain. Tightly packed aggregates ($B_2$, $A_2$) occur at small fluctuations while at high fluctuations low density of aggregates ($A_1$, $B_1$), capable of compaction under a retracting force [45], are formed. Unlike GUVs, in cells cadherin compaction can be controlled locally by modulating the long-range *cis*-interactions to induce aggregation and using short-range direct *cis*-interactions to create orderly cadherin structures [19, 24], essential for actin anchorage [6].

Having fluctuations as a control mechanism opens the intriguing possibility to manipulate adhesion by physical means, such as by changing temperature, local lipid composition, or membrane confinement, which may play a role in, for example, the placing of tight junctions close to the apical side of cells in epithelial tissues. However, changes in the physical environment often impact parameters other than membrane fluctuations, which in turn may result in interesting and useful couplings. For example, membrane fluidity was found to affect the macroscopic organization of cadherins in cells [12]. At high cadherin diffusivity (high fluidity) the adhesions formed over the entire contact zone. At low diffusivity, a ring of cadherin junctions appeared spontaneously between two adherent cells [7] and in cells binding to the substrate [12]. This different organization could be reconstituted in a model system [17, 46], where it was shown that the formation and thickness of the ring depends on the interplay between characteristic length of the path that protein makes upon entering the contact zone before forming a *trans*-bond, and the mean free path of diffusion. Fast proteins are able to reach the center of the contact zone prior to complexation, while the slow ones get recruited to adhesions at the edge of the contact zone, gradually building a coral in the form of a peripheral ring. Since fluctuations affect the complexation rates, the thickness of the ring can be modulated by the membrane.

A particularly interesting prediction of our model is the sensitivity of the two-dimensional effective binding affinity to the details of the membrane environment. The presented frame-

work may on one hand explain the significant spread in the values measured for binding energies of membrane-embedded proteins, since often the membrane environment cannot be strictly controlled [37, 47–49]. This spread, on the other hand, may be relevant physiologically, since it implies a subtle means of controlling binding-affinity of a given protein. In the context of cadherin *trans*-dimerization, we find that the effective binding affinity does not exceed $3\,k_BT$ units in the majority of the experimentally accessible phase space, making this system particularly vulnerable to small variations in experimental condition, as compared to the case of stronger ligand-receptor pairs [17, 50, 51]. It is precisely this sensitivity that makes the cadherin model ideal for probing the presented theoretical framework. Further refinement of our approach should encompass the short-range, directional *cis*-interactions, induced by the asymmetry of the cadherin *trans*-dimer which was previously identified as an important element for the lateral *cis*−oligomerization [3, 24, 52].

Given the generic physical nature of the proposed mechanisms, the regulatory potential of membrane fluctuations could be harnessed in all intra- and extracellular processes that involve the formation of inter-membrane macromolecular complexes. In fact, both thermal and active fluctuations of the plasma membrane have been identified in cells [39, 40], but their physiological significance was so far in the realm of speculations [53, 54]. Clearly, the analytical calculations as well as the $in-silico$ and $invitro$ experiments point to the regulatory role of membrane fluctuation during adhesion, both through promotion of *trans*-binding, and through generation and modulation of *cis*-interactions. We therefore propose that one of the functions of membrane fluctuations detected in cells is regulation of inter-membrane interactions.

**Data Availability Statement**

The data that support the plots within this paper and other findings of this study are available from the corresponding author upon request."

[1] Leckband, D. & Sivasankar, S. Cadherin recognition and adhesion. Curr. Opin. Cell Biol. **24**, 620–627 (2012).

[2] Lecuit, T. & Yap, A. S. E-cadherin junctions as active mechanical integrators in tissue dynamics. Nat. Cell Biol. **17**, 533–539 (2015).

[3] Wu, Y., Vendome, J., Shapiro, L., Ben-Shaul, A. & Honig, B. Transforming binding affinities from three dimensions to two with application to cadherin clustering. Nature **475**, 510–513 (2011).

[4] Volk, T., Cohen, O. & Geiger, B. Formation of heterotypic adherens-type junctions between L-CAM-containing liver cells and A-CAM-containing lens cells. Cell **50**, 987–994 (1987).

[5] Ayalon, O. et al. Spatial and temporal relationships between cadherins and pecam-1 in cell-cell junctions of human endothelial cells. J. Cell. Biol. **126**, 247–258 (1994).

[6] Strale, P.-O. et al. The formation of ordered nanoclusters controls cadherin anchoring to actin and cell–cell contact fluidity. J. Cell. Biol. **210**, 333-346 (2015).

[7] Engl, W. et al. Actin dynamics modulate mechanosensitive immobilization of E-cadherin at adherens junctions. Nat. Cell Biol. **16**, 584–591 (2014).

[8] Bello, S. M. et al. Catenin-dependent cadherin function drives divisional segregation of spinal motor neurons. J. Neurosci. **32**, 490–505 (2012).

[9] Katsamba, P. et al. Linking molecular affinity and cellular specificity in cadherin-mediated adhesion. Proc. Natl. Acad. Sci. U.S.A. **106**, 11594–11599 (2009).

[10] Gumbiner, B. M. Regulation of cadherin-mediated adhesion in morphogenesis. Nat. Rev. Mol. Cell Biol. **6**, 622–634 (2005).

[11] Jeanes, A., Gottardi, C. J. & Yap, A. S. Cadherins and cancer: How does cadherin dysfunction promote tumor progression? Oncogene **27**, 6920–6929 (2008).

[12] Biswas, K. H. et al. E-cadherin junction formation involves an active kinetic nucleation process. Proc. Natl. Acad. Sci. U. S. A. **112**, 10932–10937 (2015).

[13] Rakshit, S. & Sivasankar, S. Biomechanics of cell adhesion: How force regulates the lifetime of adhesive bonds at the single molecule level. Phys. Chem. Chem. Phys. **16**, 2211–2223 (2014).

[14] Sivasankar, S. et al. Characterizing the initial encounter complex in cadherin adhesion. Structure **17**, 1075–1081 (2009).

[15] Harrison, O. J. et al. Two-step adhesive binding by classical cadherins. Nat. Struct. Mol. Biol. **17**, 348–357 (2010).

[16] Boggon, T. J. et al. C-cadherin ectodomain structure and implications for cell adhesion mechanisms. Science **296**, 1308–1313 (2002).

[17] Fenz, S. F. & Sengupta, K. Giant vesicles as cell models. Integr. Biol. **4**, 982–995 (2012).

[18] Vendome, J. et al. Structural and energetic determinants of adhesive binding specificity in type I cadherins. Proc. Natl. Acad. Sci. U.S.A. **111**, E4175–E4184 (2014).

[19] Harrison, O. J. et al. The extracellular architecture of adherens junctions revealed by crystal structures of type I cadherins. Structure **19**, 244–256 (2011).

[20] Taveau, J.-C. et al. Structure of artificial and natural VE-cadherin-based adherens junctions. Biochem. Soc. Trans. **36**, 189–193 (2008).

[21] Hong, S., Troyanovsky, R. B. & Troyanovsky, S. M. Spontaneous assembly and active disassembly balance adherens junction homeostasis. Proc. Natl. Acad. Sci. U.S.A. **107**, 3528–3533 (2010).

[22] Ozaki, C. et al. The extracellular domains of E- and N-cadherin determine the scattered punctate localization in epithelial cells and the cytoplasmic domains modulate the localization. J. Biochem. **147**, 415–425 (2010).

[23] Hong, S., Troyanovsky, R. B. & Troyanovsky, S. M. Binding to F-actin guides cadherin cluster assembly, stability, and movement. J. Cell Biol. **201**, 131–143 (2013).

[24] Wu, Y., Jin, X., Harrison, O., Shapiro, L., Honig, B. H., & Ben-Shaul, A. Cooperativity between trans and cis interactions in cadherin-mediated junction formation. Proc. Natl. Acad. Sci. U.S.A. **107**, 17592–17597 (2010).

[25] Brasch, J. et al. Thinking outside the cell: How cadherins drive adhesion. Trends Cell Biol. **22**, 299–310 (2012).

[26] Fenz, S. F., Merkel, R. & Sengupta, K. Diffusion and intermembrane distance: Case study of avidin and E-cadherin mediated adhesion. Langmuir **25**, 1074–1085 (2009).

[27] Limozin, L. & Sengupta, K. Quantitative reflection interference contrast microscopy (RICM) in soft matter and cell adhesion. ChemPhysChem **10**, 2752–2768 (2009).

[28] Fenz, S. F. et al. Inter-membrane adhesion mediated by mobile linkers: Effect of receptor shortage. Soft Matter **7**, 952–962 (2011).

[29] Sengupta, K. & Limozin, L. Adhesion of soft membranes controlled by tension and interfacial polymers. Phys. Rev. Lett. **104**, 088101 (2010).

[30] Schmidt, D. et al. Signature of a nonharmonic potential as revealed from a consistent shape and fluctuation analysis of an adherent membrane. Phys. Rev. X **4**, 021023 (2014).

[31] Rädler, J. O. et al. Fluctuation analysis of tension-controlled undulation forces between giant vesicles and solid substrates. Phys. Rev. E **51**, 4526–4536 (1995).

[32] Seifert, U. Configuration of fluid membranes and vesicles. Adv. Phys. **46**, 13–137 (1997).

[33] Schmidt, D. et al. Coexistence of dilute and densely packed domains of ligand-receptor bonds in membrane adhesion. EPL **99**, 38003 (2012).

[34] Bazellières, E. et al. Control of cell-cell forces and collective cell dynamics by the intercellular adhesome. Nat. Cell Biol. **17**, 409–420 (2015).

[35] Bell, G. I. Models for the specific adhesion of cells to cells. Science **200**, 618–627 (1978).

[36] Dembo, M. et al. The reaction-limited kinetics of membrane-to-surface adhesion and detachment. Proc. R. Soc. London, Ser. B **234**, 55–83 (1988).

[37] Bihr, T., Seifert, U. & Smith, A.-S. Multiscale approaches to protein-mediated interactions between membranes—relating microscopic and macroscopic dynamics in radially growing adhesions. New J. Phys. **17**, 083016 (2015).

[38] Monzel, C. et al. Probing Biomembrane Dynamics by Dual-Wavelength Reflection Interference Contrast Microscopy. ChemPhysChem **10**, 2828–2838 (2009).

[39] Monzel, C. et al. Measuring fast stochastic displacements of bio-membranes with dynamic optical displacement spectroscopy. Nat. Commun. **6**, 1221–1229 (2015).

[40] Turlier, H. et al. Equilibrium physics breakdown reveals the active nature of red blood cell flickering. Nat. Phys. **12**, 513–516 (2016).

[41] Bihr, T., Seifert, U. & Smith, A.-S. Nucleation of ligand-receptor domains in membrane adhesion. Phys. Rev. Lett. **109**, 258101 (2012).

[42] Fenz, S. F. et al. Switching from Ultraweak to Strong Adhesion. Adv. Mater. **23**, 2622 (2011).

[43] Perez, T.-D. et al. Immediate-early signaling induced by E-cadherin engagement and adhesion. J. Biol. Chem. **283**, 5014–22 (2008).

[44] Adams, C. L. et al. Mechanisms of epithelial cell–cell adhesion and cell compaction revealed by high-resolution tracking of E-cadherin-green fluorescent protein. J. Cell Biol. **142**, 1105–1119 (1998).

[45] Smith, A.-S. et al. Force-induced growth of adhesion domains is controlled by receptor mobility. Proc. Natl. Acad. Sci. U.S.A. **105**, 6906–6911 (2008).

[46] Schmidt, D. et al. Crowding of receptors induces ring-like adhesions in model membranes. BBA - Mol. Cell Res. **1853**, 2984–2991 (2015).

[47] Dustin, M. L. et al. Identification of self through two-dimensional chemistry and synapses. Annu. Rev. Cell Dev. Biol. **17**, 133–157 (2001).

[48] Zhu, D.-M. et al. Analysis of two-dimensional dissociation constant of laterally mobile cell adhesion molecules. Biophys. J. **92**, 1022–1034 (2007).

[49] Hu, J., Lipowsky, R. & Weikl, T. R. Binding constants of membrane-anchored receptors and ligands depend strongly on the nanoscale roughness of membranes. Proc. Natl. Acad. Sci. U.S.A. **110**, 15283–15288 (2013).

[50] Boulbitch, A., Guttenberg, Z. & Sackmann, E. Kinetics of membrane adhesion mediated by ligand-receptor interaction studied with a biomimetic system. Biophys. J. **81**, 2743–2751 (2001).

[51] Lorz, B. G. et al. Adhesion of giant vesicles mediated by weak binding of sialyl-lewisX to E-selectin in the presence of repelling poly(ethylene glycol) molecules. Langmuir **23**, 12293–12300 (2007).

[52] Wu, Y., Honig, B. & Ben-Shaul, A. Theory and simulations of adhesion receptor dimerization on membrane surfaces. Biophys. J. **104**, 1221–1229 (2013).

[53] Zidovska, A., & Sackmann, E. Brownian motion of nucleated cell envelopes impedes adhesion. Phys. Rev. Lett. **96**, 048103 (2006).

[54] Pierres, A. et al. How cells tiptoe on adhesive surfaces before sticking. Biophys. J. **94**, 4114–4122 (2008).

**Acknowledgments**

A.-S.S. and T.B. were funded from the grant ERC StG 2013-337283 and K.S. from ERC-StG 307104FP of the European Research Council. A.-S.S and D.S. were supported by the Research Training Group 1962 at the Friedrich-Alexander-Universität Erlangen-Nürnberg. This work has partly been supported by A*MIDEX (no. ANR-11-IDEX-0001-02).

**Footnote**

*authors contributed equally

**Author Contributions**

The project was conceived and supervised by A.-S.S., K.S., U.S. and R.M. The experimental set-up was established by S.F. and K.S., and applied to the current problem by S.F. Data analysis was performed by S.F., D.S., K.S. and A.-S.S. The simulation setup was built by T.B and A.-S.S, and executed by T.B. The theoretical model was developed by D.S. and A.-S.S. with the help of T.B. and U.S. All authors contributed to the interpretation of results. The article was written by T.B., D.S., S.F. K.S. and A.-S.S.